J Arid Land (2025) 17(3): 324–336
doi: 10.1007/s40333-025-0006-0; CSTR: 32276.14.JAL.02500060

Science Press Springer-Verlag

PM_{10} dust emission in the Erenhot-Huailai zone of northern China based on model simulation

WANG Yong[1,2,3], YAN Ping[2,3*], WU Wei[4], WANG Yijiao[2,3], HU Chanjuan[1], LI Shuangquan[1]

[1] Institute of Geographical Sciences, Henan Academy of Sciences, Zhengzhou 450052, China;
[2] Faculty of Geographical Science, Beijing Normal University, Beijing 100875, China;
[3] State Key Laboratory of Earth Surface Processes and Resource Ecology, Beijing Normal University, Beijing 100875, China;
[4] College of Urban and Environmental Sciences, Hubei Normal University, Huangshi 435002, China

Abstract: The Erenhot-Huailai zone, as an important dust emission source area in northern China, affects the air quality of Beijing City, Tianjin City, and Hebei Province and human activities in this zone have a profound impact on surface dust emission. In order to explore the main source areas of surface dust emission and quantify the impacts of human activities on surface dust emission, we investigated the surface dust emission of different land types on the Erenhot-Huailai zone by model simulation, field observation, and comparative analysis. The results showed that the average annual inhalable atmospheric particles (PM_{10}) dust emission fluxes in arid grassland, Hunshandake Sandy Land, semi-arid grassland, semi-arid agro-pastoral area, dry sub-humid agro-pastoral area, and semi-humid agro-pastoral area were 4.41, 0.71, 3.64, 1.94, 0.24, and 0.14 t/hm^2, respectively, and dust emission in these lands occurred mainly from April to May. Due to the influence of human activities on surface dust emission, dust emission fluxes from different land types were 1.66–4.41 times greater than those of their background areas, and dust emission fluxes from the main dust source areas were 1.66–3.89 times greater than those of their background areas. According to calculation, the amount of PM_{10} dust emission influenced by human disturbance accounted for up to 58.00% of the total dust emission in the study area. In addition, the comparative analysis of model simulation and field observation results showed that the simulated and observed dust emission fluxes were relatively close to each other, with differences ranging from 0.01 to 0.21 t/hm^2 in different months, which indicated that the community land model version 4.5 (CLM4.5) had a high accuracy. In conclusion, model simulation results have important reference significance for identifying dust source areas and quantifying the contribution of human activities to surface dust emission.

Keywords: northern China; classification of land type; model simulation; dust emission; human disturbance

Citation: WANG Yong, YAN Ping, WU Wei, WANG Yijiao, HU Chanjuan, LI Shuangquan. 2025. PM_{10} dust emission in the Erenhot-Huailai zone of northern China based on model simulation. Journal of Arid Land, 17(3): 324–336. https://doi.org/10.1007/s40333-025-0006-0; https://cstr.cn/32276.14.JAL.02500060

1 Introduction

Surface dust emission is the process that surface dust particles are brought into the atmosphere by wind erosion. Dust, as an important source of atmospheric aerosols, is capable of altering the atmospheric radiation balance, affecting the global water cycle as well as the carbon and nitrogen cycles (Mahowald et al., 2011; Chappell et al., 2013; Kok et al., 2017; Kok et al., 2018), and having an impact on the global climatic environment and geochemical processes (Duce, 1995;

*Corresponding author: YAN Ping (E-mail: yping@bnu.edu.cn)
Received 2024-06-26; revised 2024-12-17; accepted 2025-01-07

Carslaw et al., 2010). In addition, surface dust emission can remove large amount of soil nutrients, leading to land degradation (Yan et al., 2005), and dust emission can also reduce air quality, endangering human health (Yang et al., 2017). Therefore, studies on surface dust emission are necessary. At present, mechanism, pattern, intensity, and influencing factors about surface dust emission have been comprehensively studied by field observation and indoor experiment (Ishizuka et al., 2008; Wang et al., 2021a). Many dust models were established to estimate the amount of dust emission (Shao, 2001; Kok et al., 2014). Model simulations are useful for exploring the spatial and temporal characteristics of dust emission, and play an important role in identifying dust source area, transport path, and deposition area. Although dust model can explore dust emission at different areas, a gap remains among different research scales. In recent years, much attention has been paid to the impact of human disturbance on surface dust emission (Dong et al., 1987; Cui et al., 2015), however, most of these studies are based on the plot scale with similar climate, and studies at the regional scale with different climates are relatively weak. The main reason is that it is difficult to extract human disturbance factors and assess the intensity of human disturbance at the regional scale, which leads to inconsistency and disagreement in the contribution of human disturbance to surface dust emission. Therefore, researches on dust emission at the regional scale with different climates, especially the influence of human disturbance on surface dust emission, are necessary.

Surface dust emission mainly occurs in arid and semi-arid areas in northern China (Shao et al., 2011), and has resulted in severe air pollution in the vast area of China (Liang et al., 2022). As an important dust source area in northern China, the Erenhot-Huailai zone has experienced a large amount of topsoil nutrient loss and generated a fragile ecological environment under the influence of human activities and wind erosion, which results in the air pollution of Beijing City, Tianjin City, and Hebei Province. The climates in the Erenhot-Huailai zone are arid, semi-arid, and semi-humid, and land types from north to south are desert steppe, typical steppe, agro-pastoral area, and urban-rural fringe zone, with gradually increasing precipitation, vegetation cover, and human activities. Therefore, the Erenhot-Huailai zone was selected as the study area to explore the spatial and temporal distribution characteristics of dust emission and the contribution of human activities.

Dust emission studies mainly include field observation, indoor experiment, and model simulation, in which model simulation represents an important method for studying dust emission at the regional scale (Gillette, 1988; Alfaro and Gomes, 2001; Lu and Shao, 2001; Shao, 2001; Kok et al., 2014). In recent years, the community land model version 4.5 (CLM4.5) has been widely applied in the study of surface dust emission (Shi et al., 2016; Anisimov et al., 2017). Thus, the CLM4.5 model is selected to simulate PM_{10} dust emission in the Erenhot-Huailai zone. The purpose of this study is to explore the dust emission characteristics and the contribution of human activities to surface dust emission, and to provide scientific guidance for formulating reasonable land use and management strategies, controlling and improving air quality in Beijing City, Tianjin City, and Hebei Province, and strengthening ecological environmental protection.

2 Materials and methods

2.1 Study area

The Erenhot-Huailai zone (39°30′–45°10′N, 111°10′–116°50′E; 1187 m a.s.l.) extends from the Erenhot in Inner Mongolia Autonomous Region to the Huailai Basin in Heibe Province, northern China. The study area is approximately 600 km in length and 180 km in width. It has a mid-temperate continental monsoon climate. In spring, especially in April and May, the wind is strong. The highest temperatures occur in July, and the lowest temperatures occur in January, with minimum temperatures below –25°C (Wang et al., 2016). Precipitation in the study area is uneven, and annual precipitation gradually decreases from south to north, from 500 to 200 mm. The study area is dominated by undulating hills and high plains, and the soil types primarily include brown

calcic soil, brown desert soil, chestnut soil, saline soil, and cinnamon soil. The climate in the northern part of the study area is arid and the land use types are mainly grassland (desert steppe) and sandy land. Precipitation in this area is scarce, and strong wind erosion removes large amounts of soil nutrients, resulting in infertile soil and fragile ecological environment. The climate in the central part of the study area is semi-arid and the land use types are mainly grassland (typical grassland), cultivated land, and forest land. The central part is also affected by dry weather, and wind erosion is severe. The climate in the southern part of the study area is semi-humid, and the land use types are dominated by cultivated land, followed by forest land and grassland. Due to the low-lying terrain, the area is often subject to dust deposition, resulting in relatively poor air quality. In conclusion, severe wind erosion in the study area has brought serious challenges for the development of local agriculture and animal husbandry. Additionally, the study area represents a dust transmission channel from north to south, which affects the air quality and endangers the people's health in Beijing City, Tianjin City, and Hebei Province.

2.2 Methods

Based on various influencing factors, such as wind speed, soil texture, soil water content, vegetation coverage, surface roughness, and soil freezing ratio, we used CLM4.5 model to estimate the amount of PM_{10} emitted from the study area. In addition, due to the implementation of grazing prohibition policies and the return of farmland to grassland in recent years, the vegetation conditions in the study area have been improved. Therefore, the area with high grassland coverage was considered as background area that was better protected and had less human disturbance. The dust emission amount in the background area was compared with that in the study area to analyze the impact of human activities. In addition, to explore differences between model simulation results and field observation results, we set up two dust observation instruments in the grassland of the Sonid Right Banner (43°51′21″N, 113°42′29″E) in Inner Mongolia Autonomous Region.

2.2.1 Model structure and data sources

Dust emission flux (F_j; kg/(m^2·s) in CLM4.5 model is calculated by Equation 1 (Wu et al., 2016).

$$F_j = TSf_m \alpha Q_s \sum_{i=1}^{3} M_{i,j} , \tag{1}$$

where T is the adjustment factor of the time and space resolution in the balanced dust entrainment and deposition (DEAD) model, which is 1.32×10^{-2}; S is the soil erosion factor, which is 0.02; f_m and α are the soil exposure ratio (%) and the sand initiation mass power, respectively; Q_s and $M_{i,j}$ are the horizontal flux of saltation particles (kg/(m^2·s)) and the mass fraction of different dust source modes (%), respectively; and i is the dust source mode.<

Calculation formula of soil exposure ratio (f_m) in Equation 1 is as follows:

$$f_m = (1 - f_{\text{lake}} - f_{\text{welt}})(1 - f_{\text{snow}})(1 - f_v)\left(1 - \frac{w_{\text{ice,1}}}{w_{\text{ice,1}} + w_{\text{liq,1}}}\right), \tag{2}$$

where f_{lake} is the area percentage of rivers, lakes, and reservoirs (%); f_{welt} is the area percentage of wetlands (%); f_{snow} and f_v is the snow coverage percentage (%) and vegetation coverage percentage (%), respectively; w_{ice} and w_{liq} are the ice thickness and water thickness in the soil layer (m), respectively; and $1 - \frac{w_{\text{ice,1}}}{w_{\text{ice,1}} + w_{\text{liq,1}}}$ is the soil freezing ratio.

Calculation of sand initiation mass power (α) in Equation 1 is as follows:

$$\alpha = 100\text{e}^{(13.4M\text{clay}-6.0)\ln 10}\begin{cases} M\text{clay} = \text{clay}\times 0.01 & 0\% \le \text{clay} \le 20\% \\ M\text{clay} = 20\%\text{clay}\times 0.01 & 20\% < \text{clay} \le 100\% \end{cases}, \tag{3}$$

where e is the natural logarithm and Mclay is the mass fraction of clay in the soil (%).

Calculation of horizontal flux of saltation particles (Q_s) in Equation 1 is as follows:

$$Q_s = \begin{cases} \dfrac{C_s \rho_{atm} \mu_{*s}^3}{g}\left(1-\dfrac{\mu_{*t}}{\mu_{*s}}\right)\left(1+\dfrac{\mu_{*t}}{\mu_{*s}}\right)^2 & \mu_{*t} < \mu_{*s} \\ 0 & \mu_{*t} \geq \mu_{*s} \end{cases}, \quad (4)$$

where C_s is a constant (2.61); and ρ_{atm}, μ_{*t}, μ_{*s}, and g are the atmospheric density (kg/m^3), the start-up friction wind speed of dust emission (m/s), the friction wind speed (m/s), and the gravitational acceleration (m/s^2), respectively.

Calculation of mass fraction of different dust source modes ($M_{i,j}$) in Equation 1 is as follows:

$$M_{i,j} = \frac{m_i}{2}\left[\mathrm{erf}\left(\frac{\ln\dfrac{D_{j,\max}}{D_{v,i}}}{\sqrt{2}\ln\sigma_{g,i}}\right) - \mathrm{erf}\left(\frac{\ln\dfrac{D_{j,\min}}{D_{v,i}}}{\sqrt{2}\ln\sigma_{g,i}}\right)\right], \quad (5)$$

where m_i, $D_{v,i}$, and $\sigma_{g,i}$ are the mass fraction (%), the particle size of mass median (m), and the geometric standard deviation of dust source mode i, respectively (Table 1); and $D_{j,\min}$ and $D_{j,\max}$ are the minimum and maximum particle sizes of transport mode j (m), respectively (Table 2).

Table 1 Mass fraction (m_i), particle size of mass median ($D_{v,i}$), and geometric standard deviation ($\sigma_{g,i}$) of dust source model i

Model i	m_i (%)	$D_{v,i}$ (m)	$\sigma_{g,i}$
1	3.6	0.832×10^{-6}	2.1
2	95.7	4.820×10^{-6}	1.9
3	0.7	19.380×10^{-6}	1.6

Table 2 The minimum and maximum particle sizes of particle size group j

Model j	$D_{j,\min}$ (m)	$D_{j,\max}$ (m)	Model j	$D_{j,\min}$ (m)	$D_{j,\max}$ (m)
1	0.1×10^{-6}	1.0×10^{-6}	3	2.5×10^{-6}	5.0×10^{-6}
2	1.0×10^{-6}	2.5×10^{-6}	4	5.0×10^{-6}	10.0×10^{-6}

2.2.2 Data collection

Wind speed, soil moisture (0–5 cm), and surface temperature data were obtained from China Meteorological Science Data Center. Wind speed and soil moisture data were collected at intervals of an hour. Surface temperature data were selected at four time points, namely, 02:00, 08:00, 14:00, and 20:00 (LST). We calculated the average surface temperature for each day on the basis of the temperatures at four time points. Leaf area index (LAI) was obtained from and the Atmosphere Archive and Distribution System Distributed Active Archive Center (LAADS DAAC), and determined by the data of MOD15A2H from MODIS (Moderate-resolution Imaging Spectroradiometer). LAI data were collected once every 8 d and had a spatial resolution of 1 km. Snow cover data were collected from the National Snow and Ice Data Center, and determined by the data of MOD10A2. Snow cover data were collected once every 8 d and had a spatial resolution of 500 m. The data of land use, soil texture, and land cover classification were obtained from the Resource and Environmental Science Data Center of the Chinese Academy of Sciences, the Cold and Arid Area Science Data Center, and the LAADS DAAC, with a spatial resolution of 1 km. The above data were subjected to a series of processing steps, such as projection transformation, splicing, and shearing, and the spatial resolution for all used data was 1 km. The collected period of these data was from January 2017 to December 2020.

2.2.3 Regional division and background area selection

The Erenhot-Huailai zone can be divided into four climate types, i.e., arid area, semi-arid area, dry sub-humid area, and semi-humid area (Fig. 1a). On the basis of classification of climate types, we divided the study area into six sub-areas according to land use types, i.e., arid grassland (I1),

Hunshandake Sandy Land (I2), semi-arid grassland (I3), semi-arid agro-pastoral area (I4), dry sub-humid agro-pastoral area (I5), and semi-humid agro-pastoral area (I6) (Fig. 1b). Based on the division, we considered grassland areas with high LAI values as background areas with better protection and less human disturbance, and in each land type, we selected two background areas with each background area having a diameter of 10 km (Fig. 1c). The effects of human disturbance on surface dust emission were quantified by comparing dust emissions in the background areas with those in the land type areas. Equation 6 was used to calculate the human contribution rate (P):

$$P = \frac{\sum_{n=1}^{6}(F_{In} - F'_{In}) \times S_{In}}{\sum_{n=1}^{6} F_{In} \times S_{In}}, \tag{6}$$

where F_{In} is the average dust emission fluxes from different land types (t/hm^2); F'_{In} is the average dust emission fluxes from background areas (t/hm^2); S_{In} is the areas of different land types (km^2); and n is the land use types.

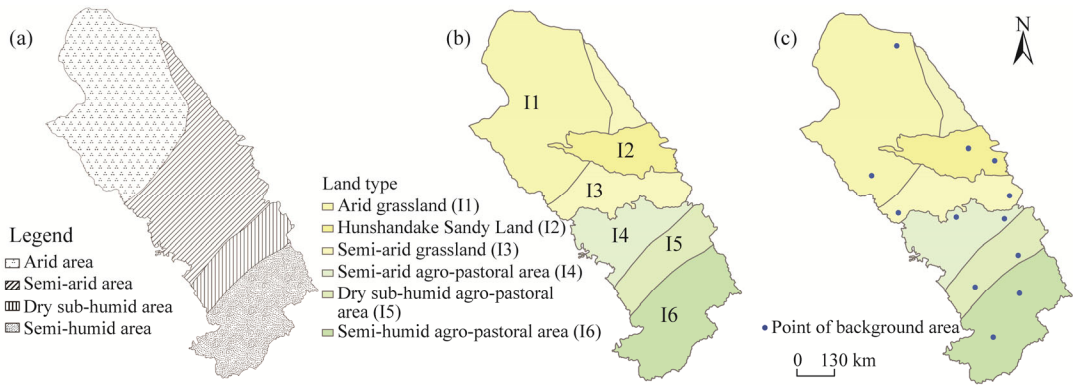

Fig. 1 Regional climate (a) and land type (b) classification and distribution of background area (c) in the Erenhot-Huailai zone, northern China

2.2.4 Field dust observation

To verify the accuracy of dust model simulation, we carried out field dust emission observations in the grassland of Sonid Right Banner (Fig. 2a). In the field observation, two DustTrak 8540 devices (TSI Incorporated, Shoreview, USA) (Fig. 2b) were installed at heights of 1.0 and 2.0 m to observe the dust emission. At the same time, two DS-2 two-dimensional ultrasonic wind speed sensors (ATMOS 22, Meter Group Inc., Pullman, USA) (Fig. 2c) were installed at the same heights to observe wind speed. The observation interval of dust and wind speed was 1 min. The observation period was from April 2018 to October 2019. Surface dust emission fluxes from the observation site were calculated by Equation 7.

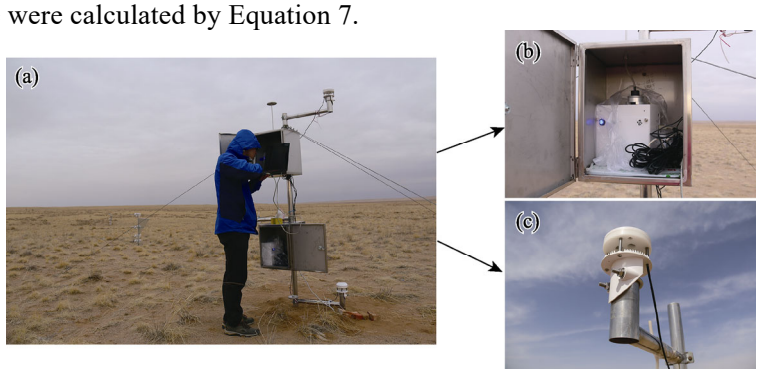

Fig. 2 Field dust observation. (a), instruments; (b), DustTrak 8540; (c), DS-2 two-dimensional ultrasonic wind speed sensor.

$$F_V = -K\mu_* \frac{Z_1 + Z_2}{2} \times \frac{C(Z_2) - C(Z_1)}{Z_2 - Z_1}, \quad (7)$$

where F_V is the vertical flux of dust emission (mg/(m^2·s)); K is the Von Karman constant, which is 0.4; μ_* is the frictional wind speed (m/s); Z_1 and Z_2 are the 1.0 and 2.0 m heights, respectively; and $C(Z_1)$ and $C(Z_2)$ are the PM_{10} concentrations at 1.0 and 2.0 m heights (mg/m^3), respectively.

3 Results

3.1 Spatial and temporal distributions of dust emission

3.1.1 Spatial distribution

Spatial distribution of PM_{10} dust emission in the study area revealed that dust emission fluxes were relatively large in the northern part of the study area and relatively small in the southern part of the study area (Fig. 3). Specifically, average PM_{10} dust emission fluxes of arid grassland and semi-arid grassland were the largest, being 4.41 and 3.64 t/hm^2, respectively (Table 3), followed by semi-arid agro-pastoral area (1.94 t/hm^2). Average PM_{10} dust emission fluxes in Hunshandake Sandy Land, dry sub-humid agro-pastoral area, and semi-humid agro-pastoral area were relatively small, with dust emission fluxes of less than 0.80 t/hm^2. The above analysis revealed that grassland and cultivated land in the arid and semi-arid areas were important dust sources. Spatial distribution characteristics of dust emission in the study area were influenced mainly by wind speed and vegetation cover. However, dust emission flux from Hunshandake Sandy Land in the northern part of the study area was relatively small, and dust emission flux from grassland around Hunshandake Sandy Land was relatively large, which indicated that soil texture of different land types also had an important influence on surface dust emission.

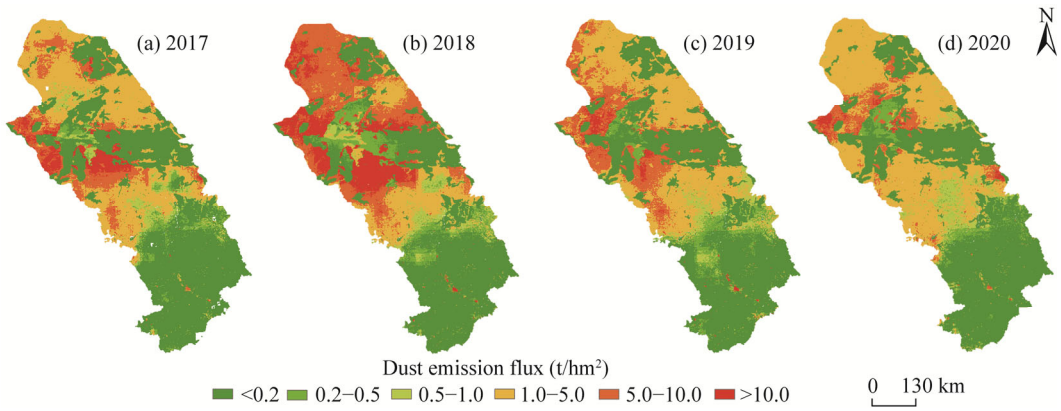

Fig. 3 Annual PM_{10} dust emission flux based on model simulation during 2017–2020. (a), 2017; (b), 2018; (c), 2019; (d), 2020.

Table 3 Average PM_{10} dust emission fluxes of different land types based on model simulation during 2017–2020

Code	Land type	Average PM_{10} dust emission flux (t/hm^2)
I1	Arid grassland	4.41
I2	Hunshandake Sandy Land	0.71
I3	Semi-arid grassland	3.64
I4	Semi-arid agro-pastoral area	1.94
I5	Dry sub-humid agro-pastoral area	0.24
I6	Semi-humid agro-pastoral area	0.14

3.1.2 Temporal distribution

According to the model simulation results (Fig. 3), dust emission fluxes in the study area varied

greatly among different years, with the largest dust emission flux occurring in 2018. Average surface dust emission flux was 4.08 t/hm^2 in 2018, and was less than 2.16 t/hm^2 in other years. High dust emission flux in 2018 was mainly related to high wind speed in the spring of that year.

Average PM_{10} dust emission flux was the largest in spring and the smallest in summer, and average PM_{10} dust emission fluxes in autumn and winter were relatively close to each other (Fig. 4). Seasonal differences in PM_{10} dust emission in the study area were mainly related to vegetation coverage, wind speed, and topsoil freezing ratio. In spring, the surface was exposed and wind speed was high (Fig. 5). Therefore, the amount of PM_{10} dust emission was high, and average PM_{10} dust flux was 1.24 t/hm^2 in spring during 2017–2020. In winter, although the surface was bare and wind speed was high, the topsoil was frozen, preventing dust release. As a result, PM_{10} dust emission flux was relatively small in winter, amounting for only 0.55 t/hm^2.

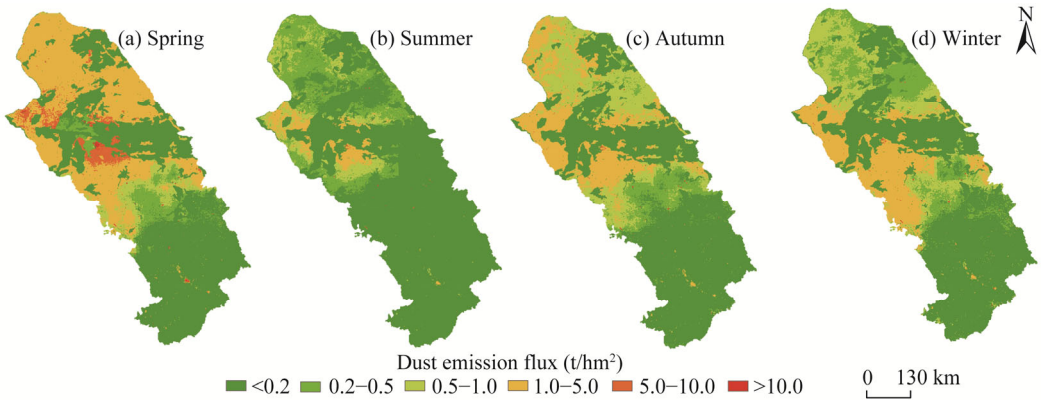

Fig. 4 Average PM_{10} dust emission flux in different seasons based on model simulation during 2017–2020. (a), spring; (b), summer; (c), autumn; (d), winter.

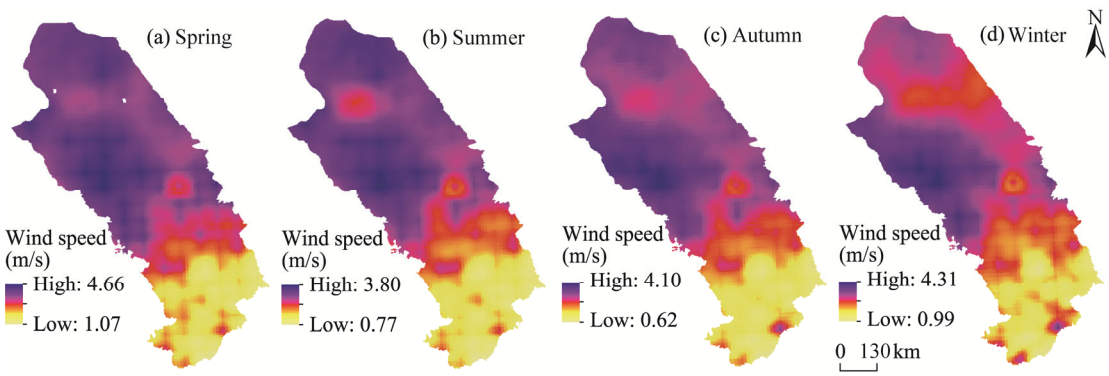

Fig. 5 Average wind speed in different seasons during 2017–2020. (a), spring; (b), summer; (c), autumn; (d), winter.

According to the average PM_{10} dust emission flux from January to December during 2017–2020 (Fig. 6), dust emission in the study area clearly changed with time. Average PM_{10} dust emission flux was stable at the lower-middle level during January–March, increased rapidly to the monthly maximum during April–May, decreased rapidly to the monthly minimum during June–September, and then increased to the lower-middle level during October–December. Monthly average PM_{10} dust emission fluxes from October to December were close to those from January to March. Average PM_{10} dust emission fluxes from the study area were 0.51 and 0.47 t/hm^2 in April and May and 0.13, 0.04, 0.02, and 0.07 t/hm^2 in June, July, August, and September, respectively. The above analyses indicated that April–May was the most active period of dust emission and that June–September was the most subdued period of dust emission in the study area.

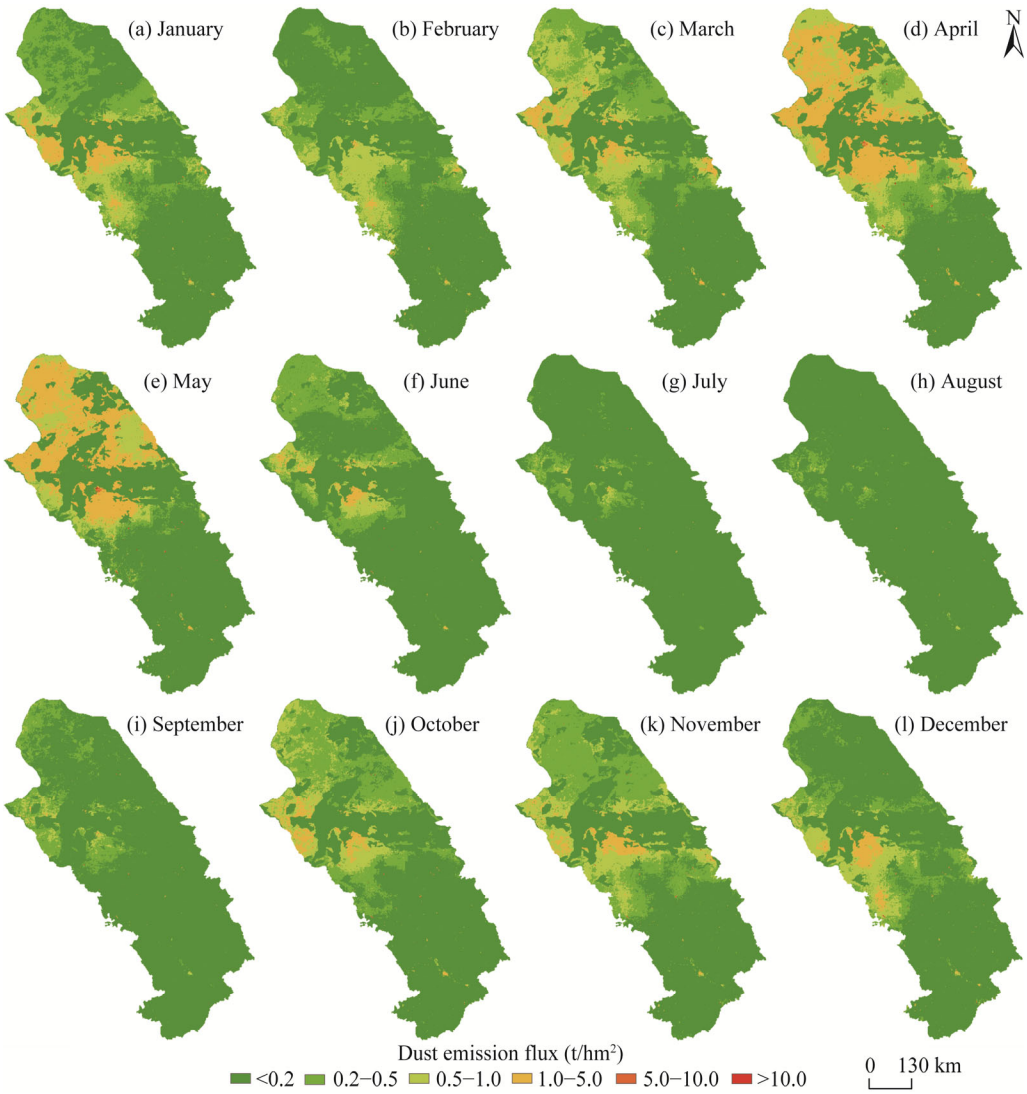

Fig. 6 Average monthly PM_{10} dust emission flux based on model simulation during 2017–2020. (a), January; (b), February; (c), March; (d), April; (e), May; (f), June; (g), July; (h), August; (i), September; (j), October; (k), November; (l), December.

3.2 Effects of human activities on surface dust emission

According to the comparative analysis of PM_{10} dust emission fluxes between land types and background areas during 2017–2020 (Fig. 7), PM_{10} dust emission fluxes of arid grassland, Hunshandake Sandy Land, semi-arid grassland, semi-arid agro-pastoral area, dry sub-humid agro-pastoral area, and semi-humid agro-pastoral area were 3.89, 3.62, 1.66, 3.18, 2.05, and 4.41 times of their background areas, respectively. In addition, the northern part of the study area is the main source area of dust emissions (arid grassland, Hunshandake Sandy Land, semi-arid grassland, and semi-arid agro-pastoral area), and PM_{10} dust emission fluxes of the main dust source were 1.66–3.89 times those of their background areas. The high dust emission in the grassland was mainly attributed to grazing, and the high dust emission in the agro-pastoral area was caused mainly by plowing and grazing. According to Equation 7, based on PM_{10} dust emission fluxes of different land types and their background areas, combined with the area occupied by each land type, we calculated the dust emission influenced by human disturbance. Results showed that PM_{10} dust emission influenced by human disturbance accounted for 58.00%

of the total PM_{10} dust emission in the study area. Since the selected background area basically represents the area with the largest grassland coverage, it can be considered that 58.00% of the surface dust emission is the maximum contribution of human disturbance in the study area.

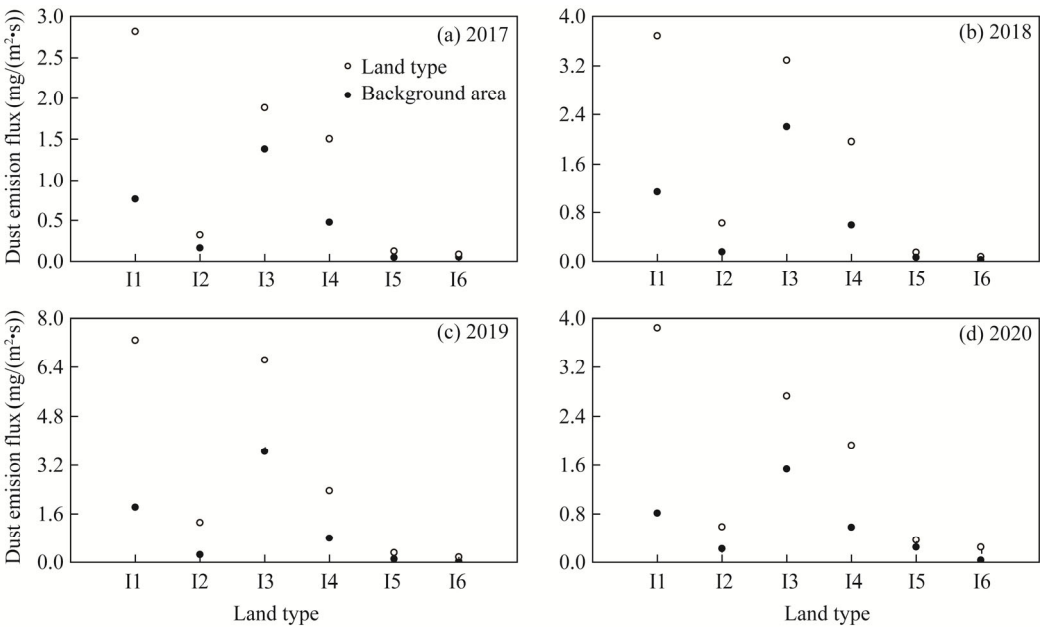

Fig. 7 Comparison of PM_{10} dust emission fluxes between land type and their background area based on model simulation during 2017–2020. (a), 2017; (b), 2018; (c), 2019; (d), 2020. I1, arid grassland; I2, Hunshandake Sandy Land; I3, semi-arid grassland; I4, semi-arid agro-pastoral area; I5, dry sub-humid agro-pastoral area; I6, semi-humid agro-pastoral area.

3.3 Model simulation verification

PM_{10} dust observation data in May and November 2018 and in February and August 2019 in the grassland of Sonid Right Banner were selected to represent dust emission of different seasons. According to comparison between model simulation and field observation (Fig. 8), PM_{10} dust emission concentrations from field observation (0.2 m and 2.0 m height) exhibited a similar trend to PM_{10} dust emission fluxes from model simulation. In addition, comparisons between observed and simulated dust emission fluxes revealed that they were close to each other (Fig. 8), with the differences ranging from 0.01 to 0.21 t/hm^2, which indicated that model simulation results could reflect the real situation of dust emission in the study area.

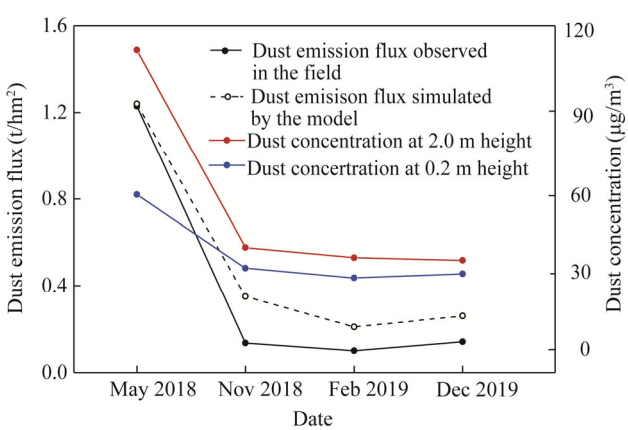

Fig. 8 Comparison of dust emission flux between field observation and model simulation

4 Discussion

4.1 PM_{10} dust emission source

PM_{10} dust emission source in the study area was mainly located in the north of dry sub-humid agro-pastoral area, and PM_{10} dust emission amount was the greatest during April–May. During April–May, the low vegetation coverage and high wind speed resulted in high PM_{10} dust emission, and studies have shown that wind and vegetation are the main factors affecting dust emission in northern China (Du et al., 2017; Meng et al., 2018; Zhang et al., 2018; Zhang et al., 2019; Lyu et al., 2021). Although PM_{10} dust emission intensity was relatively high in the north of dry sub-humid agro-pastoral area, PM_{10} dust emission flux of Hunshandake Sandy Land, which was located in the main dust source area, was relatively low, and this result was related mainly to the soil texture. Dust content in Hunshandake Sandy Land was relatively low (1.66% clay and 1.92% silt) (Wang et al., 2025), resulting in a relatively low PM_{10} dust emission, and other researchers in the field observation also showed that dust emission intensity of sand dunes was relatively low (Wang et al., 2004; Aviv et al., 2020; Wang et al., 2021b). Although PM_{10} dust emission flux in Hunshandake Sandy Land was relatively low, it was significantly greater than those in dry sub-humid agro-pastoral area and semi-humid agro-pastoral area. These findings implied that Hunshandake Sandy Land was an important potential dust source area, and other studies have shown that activated dunes can release a large amount of dust and are important dust sources (Xuan et al., 2000; Laurent et al., 2006; Sweeney et al., 2016).

4.2 Influence of human disturbance on dust emission

Many factors affect surface dust emission, including wind speed, soil moisture, vegetation coverage, soil dust content, topsoil freezing ratio, and human disturbance (Dong et al., 1987; Zender et al., 2003; Okin, 2005; Webb and Pierre, 2018; Wang et al., 2021c). Among them, human disturbance has a profound impact on surface dust emission (Du et al., 2023). In this study, human disturbances were grazing and farming. In pastoral areas, livestock grazing reduced vegetation cover and destroyed topsoil structure through gnawing, root digging, and trampling (Donovan and Monaghan, 2021). In agriculture land, farmers carry out land tilling and break up the topsoil structure. Given that land tilling completely destroyed the topsoil structure, the intensity of human interference in agriculture land was higher. Northern part located in dry sub-humid agro-pastoral area and semi-arid agro-pastoral area is dominated by grazing, and southern part is dominated by farming. The intensity of human disturbance was lower in northern part than in southern part, but the intensity of dust emission showed an opposite trend. This phenomenon is mainly due to the fact that northern part is dominated by arid and semi-arid areas, where surface ecological environment is fragile and susceptible to wind erosion. Moreover, grazing activities significantly intensify surface dust emission. However, southern part is dominated by dry sub-humid to semi-humid area, the ecosystem is relatively robust and the soil is prone to forming physical crusts despite severe soil structure degradation caused by farming. Additionally, farming practices such as leaving crop residues have further mitigated surface dust emission (Bolinder et al., 2020). Further analysis revealed that, under the same climatic condition, dust emission fluxes from different land types were 1.66–4.41 times higher than those of their background areas. Due to the relatively high dust emission in northern part, variations of total dust emission in the study area increased correspondingly, indicating that human interference had a more significant effect on dust emission in northern part. This study was carried out at the regional scale, and surface dust emission under human disturbance showed a single-digit increase. However, in previous studies at the plot scale, surface dust emission before and after human disturbance exhibited an increase on the order of several, dozens or even hundreds of times (Dong et al., 1987; Cui et al., 2015). The primary reason for this difference is that plot-scale results represent dust emission from uniformly disturbed surfaces, reflecting the outcomes under specific types of human interference, whereas regional-scale results represent dust emission from various disturbed surfaces, reflecting the overall situation of the study area. At the same time, this

difference also showed that the effects of human disturbance on surface dust emission varied greatly among different research scales.

4.3 Implications

Rational land use, implementation of ecological restoration and protection projects, and timely warning of dust storms play important roles in limiting dust emission and weakening the impact of dust emission (Wu et al., 2006; Niu et al., 2023). As shown in Figure 6, the study area experiences peak dust emission during April–May, highlighting the need to enhance early warning and preventive measures during these months. Furthermore, the monthly average dust emission flux from January to March and October to December ranges from 0.32 to 0.56 times those simulated in April and May. Therefore, timely dust warnings should also be issued during severe wind weather in these months. Spatial distribution characteristics of dust emissions indicate a relatively high intensity of dust emission in northern dry sub-humid agro-pastoral area. Therefore, it is imperative to strengthen land use management and emphasize the retention of crop residues in this area. For Hunshandake Sandy Land, the cultivation of surface biological crusts should be prioritized to prevent dune activation. For the grasslands, rational grazing practices should be adopted to minimize damage to the surface soil structure, enhance surface vegetation cover, and mitigate surface wind erosion. Furthermore, in areas experiencing severe wind erosion and significant dust emission, ecological restoration projects are essential. For example, researches have shown that forest land is effective in decreasing surface dust emission (Wang et al., 2022; Lu et al., 2024).

4.4 Limitations

In this study, surface dust emission along dust transport pathway in northern China was simulated using the CLM4.5 model, and the accuracy of simulation was verified through field observation. The results indicated that the CLM4.5 model could simulate surface dust emission with reasonable accuracy, although certain issues remained. First, due to the limitation of field observation condition, only a limited dataset spanning a few months was used for validating the model simulation, which rendered the validation insufficient. Second, in winter, the topsoil in the study area is frozen, and there should be little dust emission from the surface (Han et al., 2024). However, as shown in Figure 6, a certain amount of dust was released in December and January, suggesting that the model simulation results may be overestimated under frozen topsoil condition. These limitations highlight the need for additional field observations and the correction and improvement of model parameters related to the topsoil freezing ratio in the study area.

5 Conclusions

In this study, PM_{10} dust emission in the Erenhot-Huailai zone was simulated via the CLM4.5 model. The results showed that dust emission was mainly concentrated in spring. Northern dry sub-humid agro-pastoral area had the highest PM_{10} dust emission amount and was an important dust source area. Due to the influence of soil texture, PM_{10} dust emission of sandy land was relatively low. Dust emission in the study area was mainly affected by wind speed, vegetation coverage, soil freezing ratio, soil texture, and human disturbance, and among these factors, the effect of human disturbance on dust emission was profound. Under the influence of human disturbance, PM_{10} dust emission fluxes from the dust source areas were 1.66–3.89 times higher than those from their background areas. In addition, the effect of human disturbance on surface dust emission at the regional scale was significantly different from that at the plot scale. Therefore, further comprehensive studies on the effects of human disturbances on surface dust emission at different scales are needed.

Conflict of interest

The authors declare that they have no known competing financial interests or personal relationships that could

have appeared to influence the work reported in this paper.

Acknowledgements

This study was supported by the National Basic Research Program of China (2016YFA0601901), the Basic Scientific Research of Henan Academy of Sciences (240601083), and the Joint Fund of Henan Province Science and Technology Research and Development Program (225200810047).

Author contributions

Conceptualization: YAN Ping; Data curation: WANG Yijiao; Formal analysis: WU Wei; Methodology: WANG Yong, WU Wei; Resources: YAN Ping, WANG Yong; Software: WANG Yong, WU Wei; Writing - original draft preparation: WANG Yong; Writing - review and editing: YAN Ping, WU Wei, WANG Yijiao. All authors approved the manuscript.

References

Alfaro S C, Gomes L. 2001. Modeling mineral aerosol production by wind erosion: Emission intensities and aerosol size distributions in source areas. Journal of Geophysical Research, Atmospheres, 106(D16): 18075–18084.

Anisimov A, Tao W C, Stenchikov G L, et al. 2017. Quantifying local-scale dust emission from the Arabian Red Sea coastal plain. Atmospheric Chemistry and Physics, 17(2): 993–1015.

Aviv R, Meni B, Itzhak K. 2020. Dust emission thresholds in loess soil under different saltation fluxes. Applied Science, 10(17): 5949, doi: 10.3390/app10175949.

Bolinder M A, Crotty F, Elsen A, et al. 2020. The effect of crop residues, cover crops, manures and nitrogen fertilization on soil organic carbon changes in agroecosystems: A synthesis of reviews. Mitigation and Adaptation Strategies for Global Change, 25: 929–952.

Carslaw K S, Boucher O, Spracklen D V, et al. 2010. A review of natural aerosol interactions and feedbacks within the Earth system. Atmospheric Chemistry and Physics, 10(4): 1701–1737.

Chappell A, Webb N P, Butler H J, et al. 2013. Soil organic carbon dust emission: An omitted global source of atmospheric CO_2. Global Change Biology, 19(10): 3238–3244.

Cui M C, Lu H Y, Sweeney M, et al. 2015. PM_{10} emission flux in the Tengger Desert and Mu Us Sand field, northern China, measured by PI-SWERL. Chinese Science Bulletin, 60(17): 1621–1630.

Dong G R, Li C Z, Jin J, et al. 1987. Some results of soil erosion based on wind tunnel simulation experiment. Chinese Science Bulletin, 24(4): 297–301. (in Chinese)

Donovan M, Monaghan R. 2021. Impacts of grazing on ground cover, soil physical properties and soil loss via surface erosion: A novel geospatial modelling approach. Journal of Environmental Management, 287: 112206, doi: 10.1016/j.jenvman.2021.112206.

Du H Q, Wang T, Xue X. 2017. Potential wind erosion rate response to climate and land-use changes in the watershed of the Ningxia-Inner Mongolia reach of the Yellow River, China, 1986–2013. Earth Surface Processes and Landforms, 42(13): 1923–1937.

Du H Q, Fan Y W, Luo L H, et al. 2023. Identification of natural and anthropogenic sources and the effects of climatic fluctuations and land use changes on dust emissions variations in the Qinghai-Tibetan Plateau. Agricultural and Forest Meteorology, 340(15): 109628, doi: 10.1016/j.agrformet.2023.109628.

Duce R A. 1995. Sources, distributions, and fluxes of mineral aerosols and their relationship to climate. Aerosol Forcing of Climate, 17: 43–72.

Gillette D A. 1988. Threshold friction velocities for dust production for agricultural soils. Journal of Geophysical Research: Atmospheres, 93(D10): 12645–12662.

Han Z E, Cui W, Li J R, et al. 2024. Effect of soil moisture content on wind erosion rate of frozen aeolian sand. Journal of Desert Research, 44(1): 228–234. (in Chinese)

Ishizuka M, Mikami M, Leys J, et al. 2008. Effects of soil moisture and dried raindroplet crust on saltation and dust emission. Journal of Geophysical Research: Atmospheres, 113: D24212, doi: 10.1029/2008JD009955.

Kok J F, Mahowald N M, Fratini G, et al. 2014. An improved dust emission model-Part 1: Model description and comparison against measurements. Atmospheric Chemistry & Physics, 14(23): 13043–13061.

Kok J F, Ridley D A, Zhou Q, et al. 2017. Smaller desert dust cooling effect estimated from analysis of dust size and abundance. Nature Geoscience, 10(4): 274–278.

Kok J F, Ward D S, Mahowald N M, et al. 2018. Global and regional importance of the direct dust-climate feedback. Nature Communications, 9(1): 241, doi: 10.1038/s41467-017-02620-y.

Laurent B, Marticorena B, Bergametti G, et al. 2006. Modeling mineral dust emissions from Chinese and Mongolian deserts. Global and Planetary Change, 52(1–4): 121–141.

Liang P, Chen B, Yang X P, et al. 2022. Revealing the dust transport processes of the 2021 mega dust storm event in northern China. Science Bulletin, 67(1): 21–24.

Lu H, Shao Y P. 2001. Toward quantitative prediction of dust storms: An integrated wind erosion modelling system and its applications. Environmental Modelling & Software, 16(3): 233–249.

Lu Z Q, Dou Y Y, Wang J Z, et al. 2024. Impacts of different types of ecosystem conversion on soil wind erosion in key ecological functional zone in Inner Mongolia Autonomous Region. Bulletin of Soil and Water Conservation, 44(4): 247–256. (in Chinese)

Lyu X, Li X B, Wang H, et al. 2021. Soil wind erosion evaluation and sustainable management of typical steppe in Inner Mongolia, China. Journal of Environmental Management, 277: 111488, doi: 10.1016/j.jenvman.2020.111488.

Mahowald N, Ward D S, Kloster S, et al. 2011. Aerosol impacts on climate and biogeochemistry. Annual Review of Environment and Resources, 36: 45–74.

Meng Z J, Dang X H, Gao Y, et al. 2018. Interactive effects of wind speed, vegetation coverage and soil moisture in controlling wind erosion in a temperate desert steppe, Inner Mongolia of China. Journal of Arid Land, 10(4): 534–547.

Niu L N, Shao Q Q, Ning J, et al., 2023. The assessment of ecological restoration effects on Beijing-Tianjin Sandstorm Source Control Project area during 2000–2019. Ecological Engineering, 186: 106831, doi: 10.1016/j.ecoleng.2022.106831.

Okin G S. 2005. Dependence of wind erosion and dust emission on surface heterogeneity: Stochastic modeling. Journal of Geophysical Research: Atmospheres, 110(D11): 1371–1380.

Shao Y P. 2001. A model for mineral dust emission. Journal of Geophysical Research: Atmospheres, 106(D17): 20239–20254.

Shao Y P, Wyrwoll K H, Chappell A, et al. 2011. Dust cycle: An emerging core theme in Earth system science. Aeolian Research, 2(4): 181–204.

Shi M J, Yang Z L, Stenchikov G L, et al. 2016. Quantifying the impacts of landscape heterogeneity and model resolution on dust emissions in the Arabian Peninsula. Environmental Modelling and Software, 78: 106–119.

Sweeney M R, Lu H Y, Cui M C, et al. 2016. Sand dunes as potential sources of dust in northern China. Science China-Earth Sciences, 59(4): 760–769.

Wang G X, Tuo W Q, Du M Y. 2004. Flux and composition of wind-eroded dust from different landscapes of an arid inland river basin in north-western China. Journal of Arid Environments, 58(3): 373–385.

Wang R D, Li Q, Zhang C L, et al. 2021a. Comparison of dust emission ability of sand desert, gravel desert (Gobi), and farmland in northern China. Catena, 201: 105215, doi: 10.1016/j.catena.2021.105215.

Wang R D, Li Q, Wang R J, et al. 2021b. Influence of wind velocity and soil size distribution on emitted dust size distribution: A wind tunnel study. Journal of Geophysical Research: Atmospheres, 126(7): e2020JD033768, doi: 10.1029/2020JD033768.

Wang S S, Yu Y, Zhang X X, et al. 2021c. Weakened dust activity over China and Mongolia from 2001 to 2020 associated with climate change and land-use management. Environmental Research Letters, 16(12): 124056, doi: 10.1088/1748-9326/ac3b79.

Wang X S, Zhao W W, Liu S L, et al. 2022. Ecosystems impact on aeolian dust emissions in Inner Mongolia from 2001 to 2018. Geoderma, 422: 115938, doi: 10.1016/j.geoderma.2022.115938.

Wang Y, Yan P, Wang Y J, et al. 2025. Dust emission from different land use types based on the PI-SWERL test. Catena, 248: 108577, doi: 10.1016/J.CATENA.2024.108577.

Wang Z C, Yang J, Chen S H, et al. 2016. Impact of warmer climate on agricultural and animal husbandry climate resources in eastern Inner Mongolia. Journal of Arid Land Resources and Environment, 30(4): 132–137. (in Chinese)

Webb N P, Pierre C. 2018. Quantifying anthropogenic dust emissions. Earth's Future, 6(2): 286–295.

Wu B, Li X S, Liu W, et al. 2006. Desertification control regionalization and rehabilitation countermeasures of source area of the sand and dust endangering Beijing-Tianjin. Scientia Silvae Sinicae, 42(10): 65–70. (in Chinese)

Wu C L, Lin Z H, He J X, et al. 2016. A process-oriented evaluation of dust emission parameterizations in CESM: Simulation of a typical severe dust storm in East Asia. Journal of Advances in Modeling Earth Systems, 8(3): 1432–1452.

Xuan J, Liu G L, Du K. 2000. Dust emission inventory in Northern China. Atmospheric Environment, 34(26): 4565–4570.

Yan H, Wang S Q, Wang C Y, et al. 2005. Losses of soil organic carbon under wind erosion in China. Global Change Biology, 11(5): 828–840.

Yang Y, Russell L M, Lou S J, et al. 2017. Dust-wind interactions can intensify aerosol pollution over eastern China. Nature Communications, 8(1): 15333, doi: 10.1038/ncomms15333.

Zender C S, Newman D, Torres O. 2003. Spatial heterogeneity in aeolian erodibility: Uniform, topographic, geomorphic, and hydrologic hypotheses. Journal of Geophysical Research: Atmospheres, 108(D17): 4543, doi: 10.1029/2002JD003039.

Zhang G F, Azorin-Molina C, Shi P J, et al. 2019. Impact of near-surface wind speed variability on wind erosion in the eastern agro-pastoral transitional zone of Northern China, 1982–2016. Agricultural and Forest Meteorology, 271: 102–115.

Zhang H Y, Fan J W, Cao W, et al. 2018. Response of wind erosion dynamics to climate change and human activity in Inner Mongolia, China during 1990 to 2015. Science of the Total Environment, 639: 1038–1050.